Applied Surface Science 425 (2017) 121–129

Contents lists available at ScienceDirect

Applied Surface Science

journal homepage: www.elsevier.com/locate/apsusc

Full Length Article

Nanoscale domains of ordered oxygen-vacancies in $LaCoO_3$ films

Guiju Liu[a,1], Xiaotian Li[a,1], Yiqian Wang[a,*], Wenshuang Liang[a], Bin Liu[a], Honglei Feng[a], Huaiwen Yang[b], Jing Zhang[b], Jirong Sun[b]

[a] College of Physics & The Cultivation Base for State Key Laboratory, Qingdao University, No. 308 Ningxia Road, Qingdao, 266071, People's Republic of China
[b] Beijing National Laboratory for Condensed Matter Physics, Institute of Physics, Chinese Academy of Sciences, Beijing, 100080, People's Republic of China

ARTICLE INFO

Article history:
Received 23 January 2017
Received in revised form 19 June 2017
Accepted 29 June 2017
Available online 5 July 2017

Keywords:
$LaCoO_3$ epitaxial film
HRTEM
Dark stripes
Oxygen vacancy ordering
Ferromagnetism

ABSTRACT

High-quality $LaCoO_3$ (LCO) thin films were epitaxially grown on $SrTiO_3$ (STO), $(La,Sr)(Al,Ta)O_3$ (LSAT) and $LaAlO_3$ (LAO) substrates using pulsed laser deposition technique. Nanoscale domains with either horizontally or vertically modulated dark stripes are observed in the LCO films on STO and LSAT substrates, whereas only horizontally-modulated domains are found in the films on LAO substrate. The domain sizes and directions strongly depend on the strain state of the films due to lattice mismatch between film and substrate. The lattice strains in the films are mainly relaxed through change of the domain directions. The oxygen deficiency of the films has been revealed by X-ray photoelectron spectroscopy. As confirmed by high-angle annular dark field (HAADF) observations and high-resolution transmission electron microscopy (HRTEM) image simulations, the modulated dark stripes stem from oxygen-vacancy ordering, which causes local lattice expansion. The saturation magnetization increases with the tensile strain in the films. The ferromagnetic character is correlated with the oxygen deficiency, strain state and vertically modulated domains.

1. Introduction

$LaCoO_3$ (LCO) is a very interesting material that can work as a cathode for solid-oxide fuel cells and batteries [1], a colossal magnetoresistance material [2], and a magnetic recording medium [3]. Recently, LCO epitaxial film has attracted significant attention due to its interesting ferromagnetism (FM) and spin-state transition [4,5]. The physical properties of thin films are greatly affected by lattice strain, defect structure and oxygen non-stoichiometry. The epitaxial strain in LCO films imposed by substrates could influence their magnetic properties [6]. The variation in oxygen content of the films could result in changes of lattice parameters, which are expected to influence orbital ordering and spin state transition and further affect the magnetic and transport properties of perovskite oxide thin films [7]. It is known that oxygen vacancies play an important role in magnetic properties [8] and ionic conductivity [9,10]. In our recent work, we found that the oxygen vacancies restrain the spin polarization of Co cations and further depress the magnetism of $La_{0.67}Sr_{0.33}CoO_{3-\delta}$ films [8]. In other $LaCoO_3$-based perovskite oxide films, the existence of oxygen vacancies could destruct double-exchange interaction between Co—O—Co bonds, which leads to a transformation from ferromagnetic metal to non-magnetic insulator [9,10]. But in other oxide films, the effects of oxygen vacancy on the magnetic and transport properties may be different. For instance, Wang et al. [11] declared that in $SrMnO_{3-\delta}$ films oxygen vacancy can affect the valence states of Mn ions, which results in double exchange between Mn^{3+} and Mn^{4+} and ferromagnetic properties. In $La_{2/3}Sr_{1/3}MnO_3$ films, oxygen vacancies were found to induce degraded ferromagnetic and transport properties [12]. Up to now, the effect of oxygen vacancies on the magnetic properties of LCO films is not fully understood and needs further investigation.

Very recently, high-quality epitaxial LCO films have been grown on various substrates, exhibiting strain-dependent microscopic lattice modulations [13–15]. Both experimental and theoretical efforts have been made to explore the nature of the spin state transition and FM [16–18]. However, the underlying physics of the FM and spin state transition remains elusive. For instance, combining high-angle annular dark field (HAADF) images, electron energy-loss spectroscopy (EELS) and density functional theory calculations, Choi et al. [19] declared that the dark stripes in epitaxial LCO thin films on different substrates stemmed from the ordering of high spin (HS) Co^{3+} ions. However, Biškup et al. [20] believed that the dark stripes in the HAADF images of the LCO films correspond to significantly dilated La–La distances, and the ordering of oxygen

* Corresponding author.
E-mail address: yqwang@qdu.edu.cn (Y. Wang).
[1] These authors contribute equally to this work.

http://dx.doi.org/10.1016/j.apsusc.2017.06.315
0169-4332/

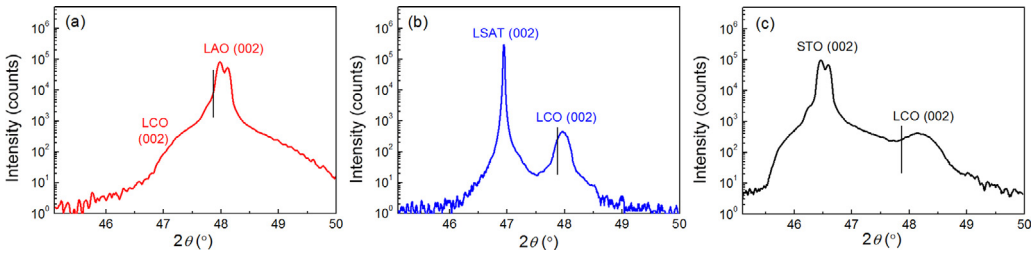

Fig. 1. XRD patterns of the 002 peaks showing the out-of-plane lattice parameters of LCO films on (a) LAO, (b) LSAT and (c) STO substrates, respectively.

vacancies is responsible for the occurrence of FM and dark stripes. In addition, they declared that the oxygen vacancy ordering can stabilize a long-range ferromagnetic ordering in $LaCoO_{3-\delta}$ films [21]. However, a reasonable explanation how these defects stabilize the long-range ferromagnetic ordering is still lacking. Moreover, the exact origin of the dark stripes in the LCO films has not been unveiled.

In this paper, we presented a systematic investigation on the atomic and electronic structures of the LCO films grown on different substrates. Nanoscale domain structures with different sizes and directions were observed using high-resolution transmission electron microscopy (HRTEM) and HAADF. The nature of modulated dark stripes was explored based on the simulation of the HRTEM images and the underlying mechanism for the FM was investigated through the correlation of magnetism, strain and microstructure.

2. Experimental

High-quality epitaxial LCO films were grown on various substrates of $LaAlO_3$ (LAO), $(La,Sr)(Al,Ta)O_3$ (LSAT), and $SrTiO_3$ (STO) using pulsed laser deposition (PLD) with a 248 nm KrF laser. During the deposition process, the substrate temperature was kept at 720 °C and the oxygen pressure at 50 Pa. The film thickness, ~15 nm, was determined by the number of laser pulses. After deposition, the films were annealed for 15 min under an oxygen pressure of 1 bar, and then cooled down to room temperature.

Specimens for transmission electron microscopy (TEM) observations were prepared in cross-sectional orientation ([010] zone-axis for STO, LSAT and LAO substrates) using conventional techniques of mechanical polishing and ion thinning. The ion thinning was performed using a Gatan model 691 precision ion polishing system (PIPS) with low voltage. To enhance the performance and capabilities of the PIPS, a liquid N_2 cooling option is available. Bright field (BF) imaging, selected-area electron diffraction (SAED) patterns and HRTEM images were obtained using a JEOL JEM 2100F TEM operating at 200 kV. To avoid any beam damage to the samples, the exposure time is set to be less than 1 s. HAADF investigation was carried out using a JEOL JEM-ARM200F microscope with double Cs correctors. X-ray photoemission microscopy (XPS) was recorded with Omicron 0571 spectrometer using Mg Kα (1253.6 eV) and a spot size of 800 μm. Magnetic measurements were conducted on a Quantum Design vibrating-sample magnetometer (VSM–SQUID) with a temperature of 10 K. The applied magnetic field was parallel to the sample surface as well as the current direction. The zero-field-cooling (ZFC) and field-cooling (FC) magnetization curves were measured under an applied field of 0.05 T in a temperature range of 10–300 K using a VSM–SQUID. All the magnetization data were processed to separate the substrate influence. For thermal magnetization, the contribution of the substrate was directly subtracted from the total magnetization. For isothermal magnetization, the substrate influence was deducted through high field linear fitting.

Table 1
The out-of-plane lattice parameters for LCO films and substrates.

	a_c of substrate (Å)	a_c of LCO film (Å)
LCO/LAO	3.786	3.843
LCO/LSAT	3.866	3.789
LCO/STO	3.905	3.773

3. Results and discussion

LCO films were epitaxially grown on different substrates, which can be confirmed by X-ray diffraction (XRD). Fig. 1 shows the XRD patterns of the 002 peak, which reveals information regarding the out-of-plane lattice parameters as a function of the substrate-film lattice mismatch. The straight line in Fig. 1 demonstrates the (002) peak position of bulk LCO (a_c = 3.805 Å). Compared to bulk LCO, the (002) reflection of the film on LAO substrate shifts to small angles, as shown in Fig. 1(a), indicating that the film experiences a compressive strain with an out-of-plane lattice expansion. On contrary, for the films grown on LSAT and STO, the (002) reflections of the film shift to large angles, as shown in Fig. 1(b) and (c), suggesting that the film suffers a tensile strain with an out-of-plane lattice contraction. Note that the 002 peak of LCO film grown on LAO is not obvious in comparison with that of LCO films grown on STO and LSAT. To identify the 002 peak positions for both LCO film and LAO substrate, peak-differentiating and imitating was adopted to analyze the XRD pattern in Fig. 1(a), as shown in Fig. S1 in the Supplementary material. Table 1 summarizes the out-of-plane lattice parameters of films and substrates, measured from the XRD patterns. It can be seen that for the LCO films grown on LAO, the out-of-plane lattice parameter is larger (~3.84 Å) than that on LSAT and STO. The out-of-plane lattice parameters for films on LSAT and STO are measured to be ~3.79 Å and ~3.77 Å, smaller than that of bulk LCO.

To obtain further information about the structure, we performed TEM examinations of the LCO films. Fig. 2(a), (c) and (e) show the typical BF TEM images, along the pseudo-cubic [010] zone-axis of the LCO films grown on LAO, LSAT and STO substrates, respectively. The distinct interfaces between films and substrates (marked by dashed lines) can be clearly seen. Interestingly, both horizontal and vertical modulations are observed in the LCO films on LSAT and STO, whereas there are only horizontal modulations in the film on LAO. Moreover, the domain sizes are different in the films grown on LSAT and STO. Fig. 2(b), (d) and (f) are the SAED patterns obtained from the LCO films grown on LAO, LSAT and STO, respectively. The strong reflections in the SAED patterns are associated with the perovskite structure of LCO, whereas the weak reflections (indicated by arrows) originate from a superstructure with a periodicity of $3a_0$, where a_0 is the lattice constant of LCO. Moreover, for the LCO/STO film, the weak diffraction spots from the vertical stripes are elongated, suggesting the existence of incommensurate modulations (Fig. 2(f)).

To clarify the nature of domain structures, systematic TEM investigations were carried out. Fig. 3(a) and (b) are typical TEM

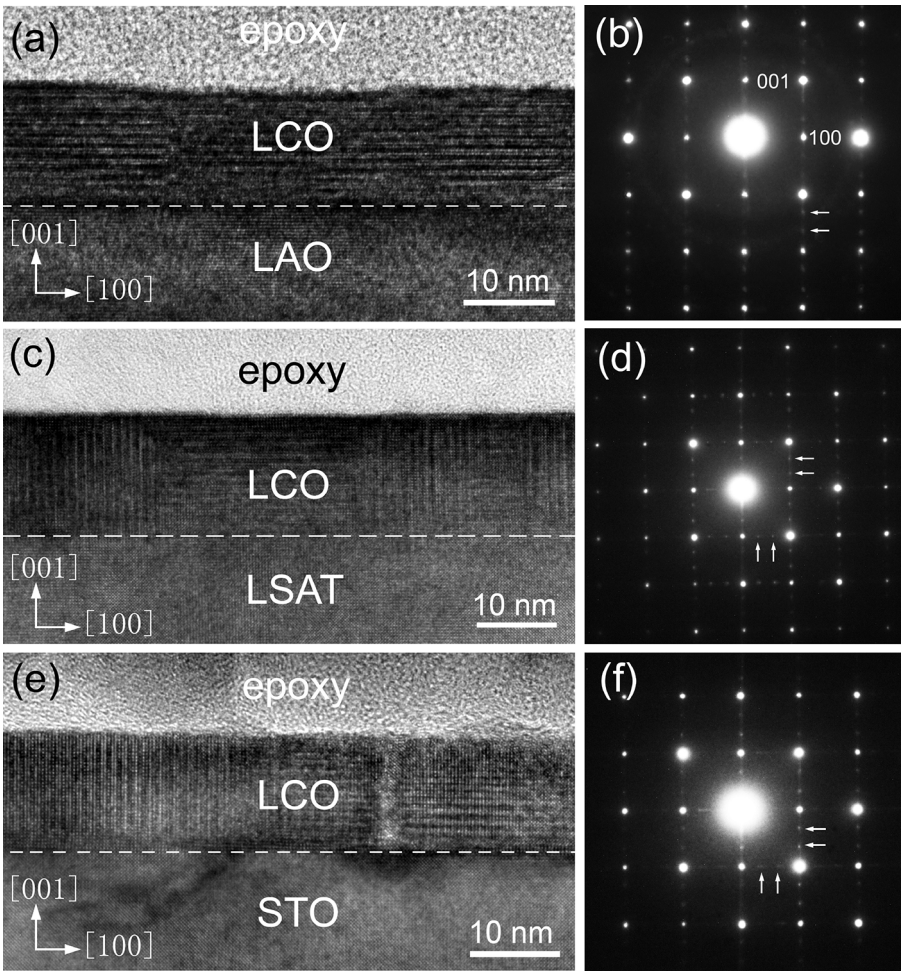

Fig. 2. Cross-sectional TEM images of LCO films grown on (a) LAO, (c) LSAT, and (e) STO. (b), (d) and (f) Corresponding SAED patterns taken from the LCO films.

images of LCO/LSAT films taken under a two-beam condition with **g** = 001 and **g** = 100, respectively. Fig. 3(c) and (d) are typical TEM images of LCO/STO films taken under a two-beam condition with **g** = 001 and **g** = 100, respectively. For **g** = 100, vertical domain structures can be clearly observed, while for **g** = 001, horizontal domain structures can be obviously seen. The average domain dimension is measured to be 25.10 nm for LCO/LSAT and 13.32 nm for LCO/STO. The LCO films are subjected to tensile strain on the LSAT and STO substrates. The lattice mismatch is ~1.68% for LCO/LSAT which is smaller than that for LCO/STO film (~2.56%). It reveals that the domain size decreases with the increase of the lattice mismatch.

To correlate the domain dimension with strain state and lattice mismatch, we analyzed the different strain states and lattice mismatches in the films on three substrates. The films grown on LAO are under in-plane compressive strain, whereas films grown on STO and LSAT are under in-plane tensile strain. For the film under compressive strain (LCO/LAO), only horizontal domain structures were observed. However, for the films under tensile strain (LCO/STO and LCO/LSAT), not only horizontal but also vertical domain structures were found. As the degree of tensile strain increases, more vertical domain structures appear, and the domain dimension decreases, which can be clearly seen from Fig. 3. This means that the domain structures and their changes in the orientation of stripes are associated with lattice strain. In addition, in the epitaxial films, the critical thickness values are 1.8 nm, 3.4 nm and 26 nm for the LCO films grown on STO, LSAT and LAO, respectively [19]. For the 15-nm-thick LCO film grown on LAO substrate, the lattice mismatch is relatively small (−0.42%), and the film thickness is smaller than the critical thickness. The strain caused by lattice mismatch can be accommodated by elastic deformation and no domain structure will form (Fig. 2(a)). However, the lattice mismatch is considerably large for LCO/LSAT (1.68%) and LCO/STO (2.56%). In these two cases, the film thickness is larger than the critical thickness. Thus, the strain generated by the lattice mismatch has to be relaxed by the formation of misfit dislocations at the interfacial regions. It was reported, besides the formation of misfit dislocations, perovskites often show elastic, pseudo-periodic twinning, antiphase domains and phase transition to relieve epitaxial strain [22]. However, in our case, no misfit dislocations or other defects, which can be readily imaged by HRTEM, are observed in the LCO films. Either vertical or horizontal domains are found in these films, and the domain size decreases with increasing lattice mismatch (Fig. (3)). Thus, we suggest that the interfacial strain is mainly relaxed through the formation of domain structures with different directions. Based on the analysis above, we found that the domain size is strongly dependent on the lattice strain in the films. The relationship between domain dimension (d) and lattice mismatch (f) can be expressed by

$$d = \frac{1}{f} \times a_s \tag{1}$$

where a_s refers to the lattice constant of the substrate. The domain dimensions (d) are calculated to be 90.21 nm, 23.04 nm and 15.25 nm for the LCO films grown on LAO, LSAT and STO, respectively, consistent with those measured from the TEM images in Figs. 2 and 3.

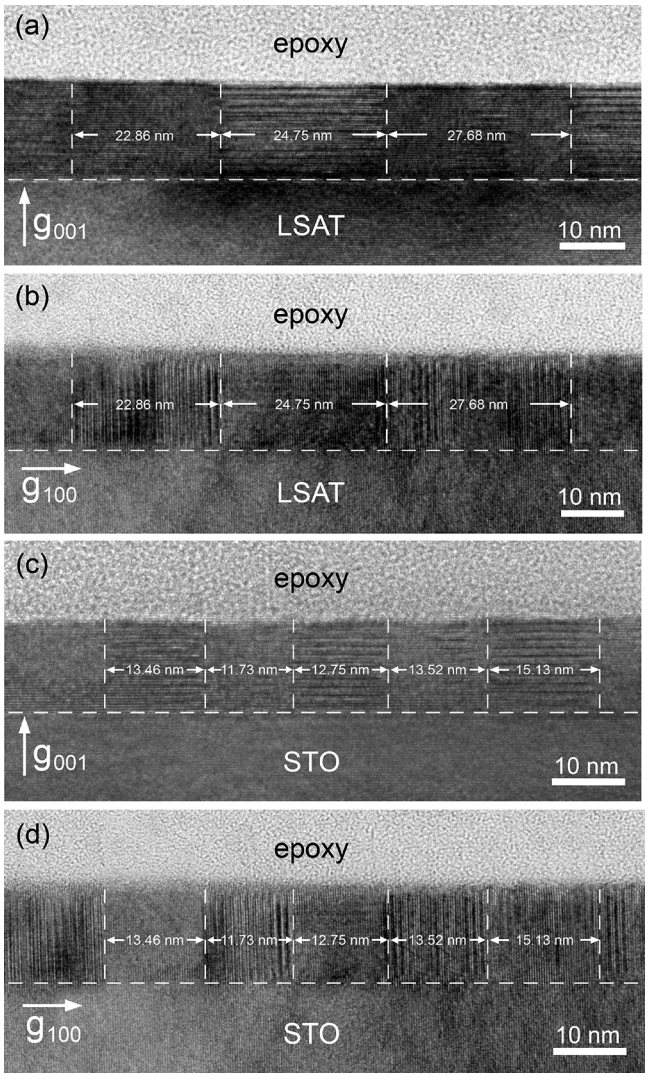

Fig. 3. Cross-sectional TEM images of LCO/LSAT films taken near the [010] zone-axis with a diffraction vector of (a) **g** = 001 and (b) **g** = 100. Cross-sectional TEM images of LCO/STO films taken near the [010] zone-axis with a diffraction vector of (c) **g** = 001 and (d) **g** = 100.

Fig. 4 shows the typical [010] zone-axis HRTEM images of the LCO films grown on different substrates. Perpendicular or parallel dark stripes in the films can be clearly seen. The intensity profiles along the green and red lines drawn in Fig. 4 are shown in the insets, where the black lines indicate the positions of dark stripes. Based on the analysis of the intensity profiles, we assure that evident modulated structures exist in the LCO films. For the films grown on LAO and LSAT, the modulations are commensurate, with a periodicity of $3a_0$, as shown in Fig. 4(a) and (b). However, the modulations are incommensurate in LCO/STO, with a periodicity of $3a_0$ or $4a_0$ as confirmed by the SAED pattern in Fig. 2(f). Similar modulated stripes have also been observed in Sr-doped cobaltite films, which are attributed to the ordering of oxygen vacancies [8,9,23,24], cations [23], and even ferroelastic structural twinning [25,26]. Recently, Kwon [13], Choi [19], Biškup [20] and Mehta [21] et al. found similar dark stripes in the HAADF images and attributed them to HS state of Co^{3+} [13,19] and oxygen vacancies [20,21], respectively. However, they only observed the modulations with vertical stripes in the LCO/STO and LCO/LSAT films. In our work, dark stripes perpendicular and parallel to the interface are observed in these two films. For the LCO/LAO film only horizontal dark stripes are found, which is consistent with the report of Choi et al. [19].

XPS analyses were performed to investigate the chemical composition of the LCO films grown on different substrates. Fig. 5(a–c) show the XPS spectra of La 3*d*, O 1*s* and Co 2*p* for the LCO films on STO, respectively. In Fig. 5(a), the two peaks at binding energies of 835.03 eV and 851.67 eV are associated with La $3d_{5/2}$ and La $3d_{3/2}$, respectively. Each one shows two components, which is attributed either to energy loss phenomena (shake-up satellites) induced by intense O $2p \rightarrow$ La $4f$ charge transfer events or to strong final state mixing of electronic configurations [27]. In Fig. 5(b), the lower binding-energy peak at 528.51 eV is assigned to intrinsic lattice site oxygen, and the higher binding-energy peak at 530.53 eV is attributed to adsorbed oxygen. In Fig. 5(c), the $2p_{3/2}$ and $2p_{1/2}$ peaks are located at 779.73 and 795.04 eV, respectively, separated by an energy of 15.31 eV. The smaller intense peak at about 789.35 eV is a satellite peak associated with the Co ion [28,29], which suggests that divalent cobalt species are present in the LCO films on STO. The standard peaks [30] provide a reference for the fitting of Co 2*p* spectrum, and Table 2 summarizes the peak positions deduced from Gaussian-Lorentzian calculations. Higher binding energy peaks correspond to Co^{2+} ion, whereas lower binding energy peaks correspond to Co^{3+} ion in the LCO film [31,32]. Through the calculation of Co^{2+}/Co^{3+} ratio, we deduced that the average oxygen deficiency is about 10%, consistent with the estimated content of oxygen vacancy (~9.8%). Although the XPS can only detect information within the surface depths of about 8–10 nm [33], the film thickness is only about 15 nm, and the dark stripes are distributed evenly over the entire film thickness, as shown in Fig. 2(c). Therefore, in the whole LCO film, the concentration of oxygen vacancy can be considered to be the same (10%), and the chemical formula of LCO film grown on STO is determined to be $LaCoO_{2.7}$. For the LCO films grown on LSAT and LAO, XPS analyses demonstrate similar results of oxygen deficiency (Fig. S2 in Supplementary material).

Figs. 6(a) and 7(a) are enlarged HRTEM images of vertically and horizontally modulated dark stripes, respectively. It is usually acknowledged that from the HRTEM images, it is hard to observe spin-state ordering but easy to detect the ordering of oxygen vacancies, for example, for Sr-doped cobaltite films [8–10,34,35]. Figs. 6(b) and 7(b) show the HAADF images of the ordered domains. In the HAADF images the intensity of every atomic column is approximately proportional to $Z^{1.67}$, so the brightest features are columns of La and the next brightest features are columns of Co. One Co—O plane exhibits a significantly dark contrast and the other two Co—O planes demonstrate grey contrast. This periodical sharp decrease in the intensity of Co—O planes indicates that there is less high-angle scattering, which can be attributed to loss of atoms from the column [15]. To clarify the origin of the modulated stripes in the LCO films, we mapped out the in-plane interatomic spacing (red lines) and

Table 2
Binding energy of Co 2*p* obtained from Fig. 5c (MP and SP refer to the main peak and satellite peak, respectively. FWHM refers to full width at half maximum.).

Spin-orbit	Species	Binding Energy (eV)	Area	FWHM (eV)
$2p_{3/2}$ (MP)	Co^{3+} (24.36%)	779.22	28006.15	1.52
	Co^{2+} (41.05%)	780.54	47198.78	3.39
$2p_{3/2}$ (SP)	Co^{2+} (4.66%)	789.35	5353.15	2.82
$2p_{1/2}$ (MP)	Co^{3+} (15.37%)	794.38	17664.54	1.95
	Co^{2+} (14.56%)	796.36	16743.44	2.89

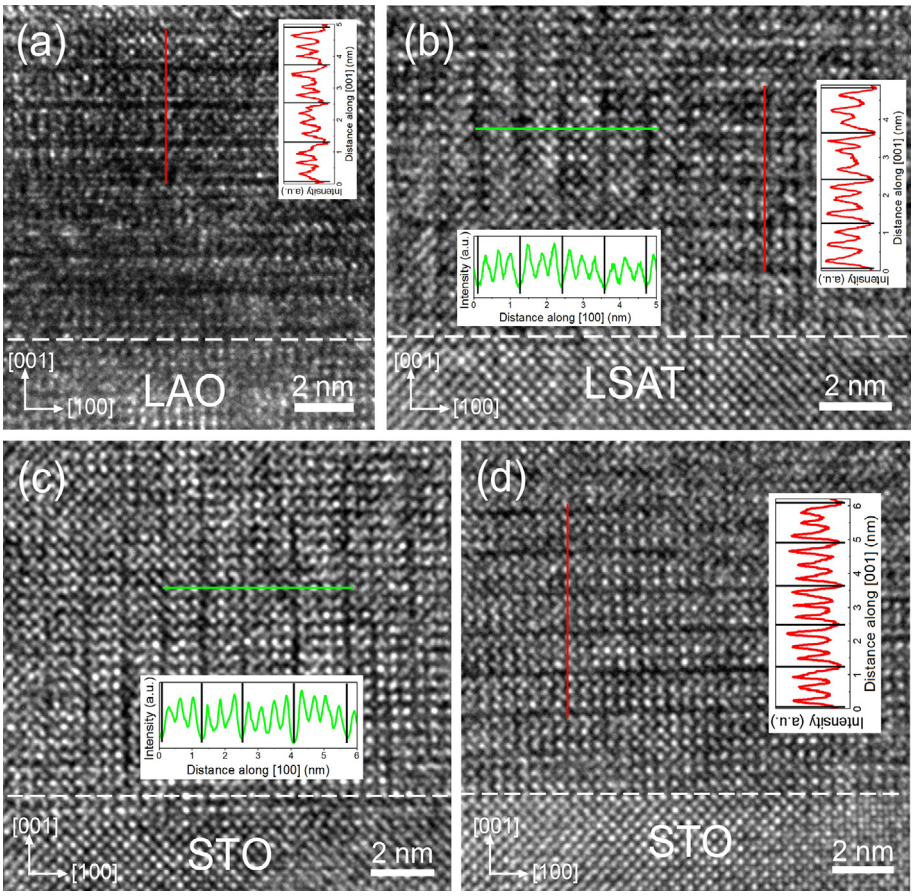

Fig. 4. Typical [010] zone-axis HRTEM images of (a) LCO/LAO and (b) LCO/LSAT. Typical [010] zone-axis HRTEM images of LCO/STO with (c) vertical modulations and (d) horizontal modulations. Insets show the intensity profiles for the red and green lines drawn in the HRTEM images. (For interpretation of the references to colour in this figure legend, the reader is referred to the web version of this article.)

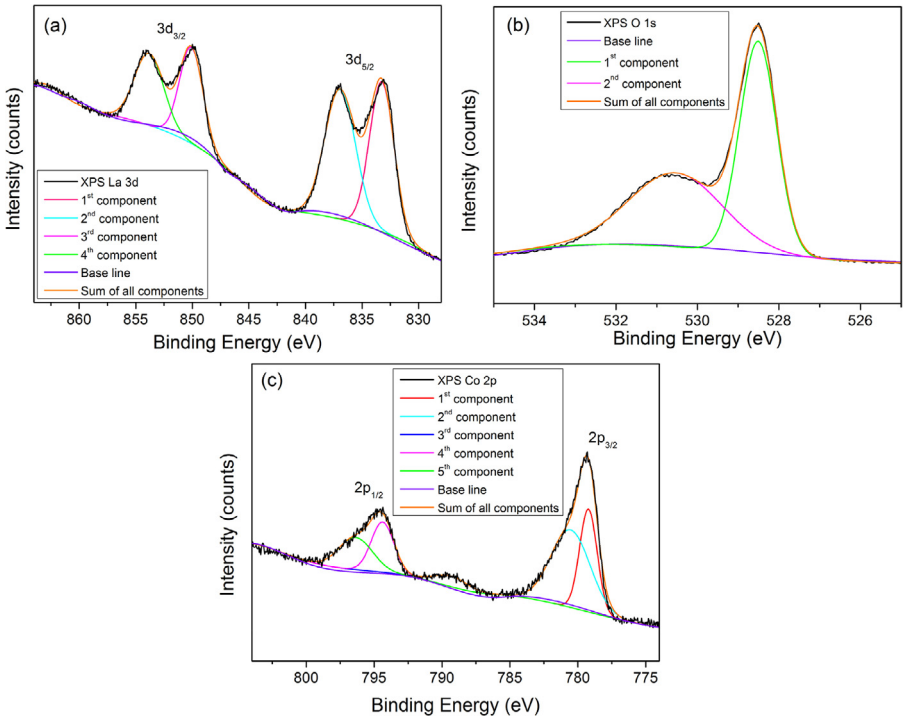

Fig. 5. XPS spectra of (a) La 3*d*, (b) O 1*s*, and (c) Co 2*p* for the LCO/STO film.

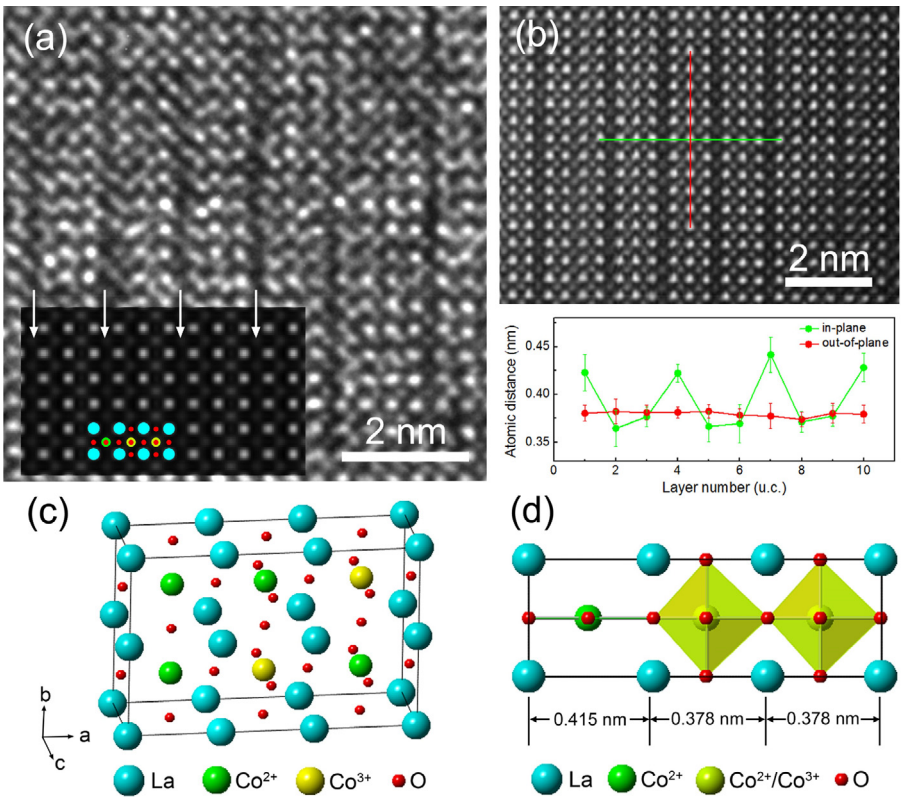

Fig. 6. (a) Typical HRTEM image of LCO films with vertical modulations, inset is the simulated HRTEM image with $\Delta f = -15.0$ nm and $t = 22.7$ nm. (b) Typical HAADF image of the LCO film and in-plane/out-of-plane atomic distances between the La atoms. (c) Atomic model for the vertical modulations in the LCO films. (d) Schematic diagram of the atomic projection along *b* axis.(For interpretation of the references to colour in the text, the reader is referred to the web version of this article.)

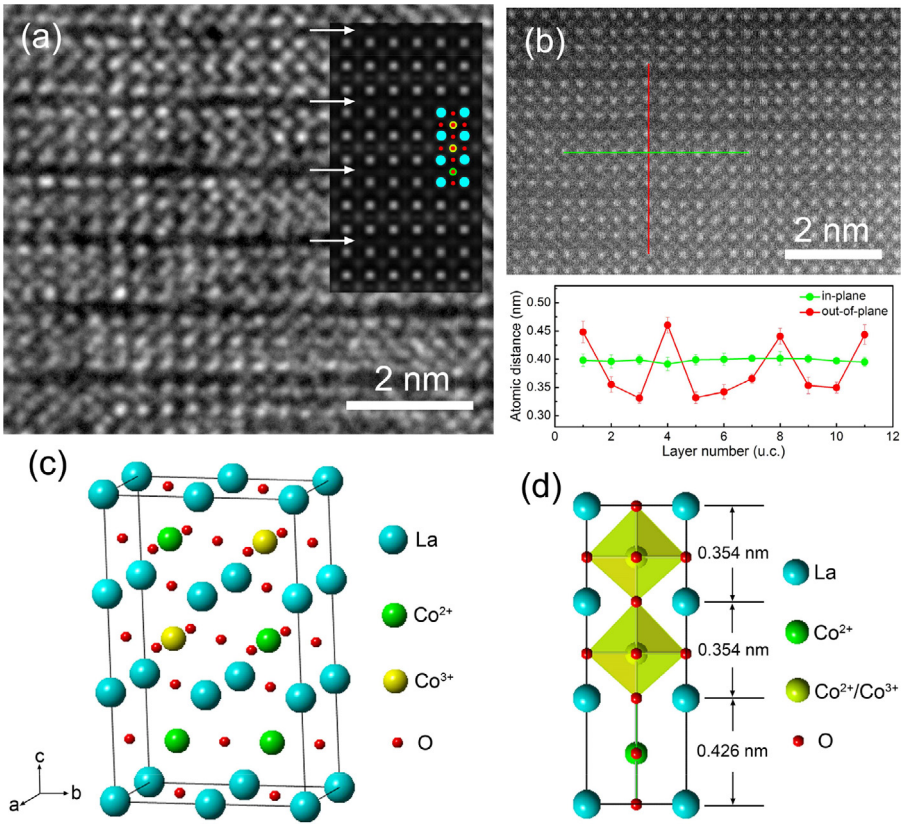

Fig. 7. (a) Typical HRTEM image of LCO films with horizontal modulations, inset is the simulated HRTEM image with $\Delta f = -15.0$ nm and $t = 24.6$ nm. (b) Typical HAADF image of the LCO film and in-plane/out-of-plane atomic distances between the La atoms. (c) Atomic model for the horizontal modulations in the LCO films. (d) Schematic diagram of the atomic projection along *b* axis.

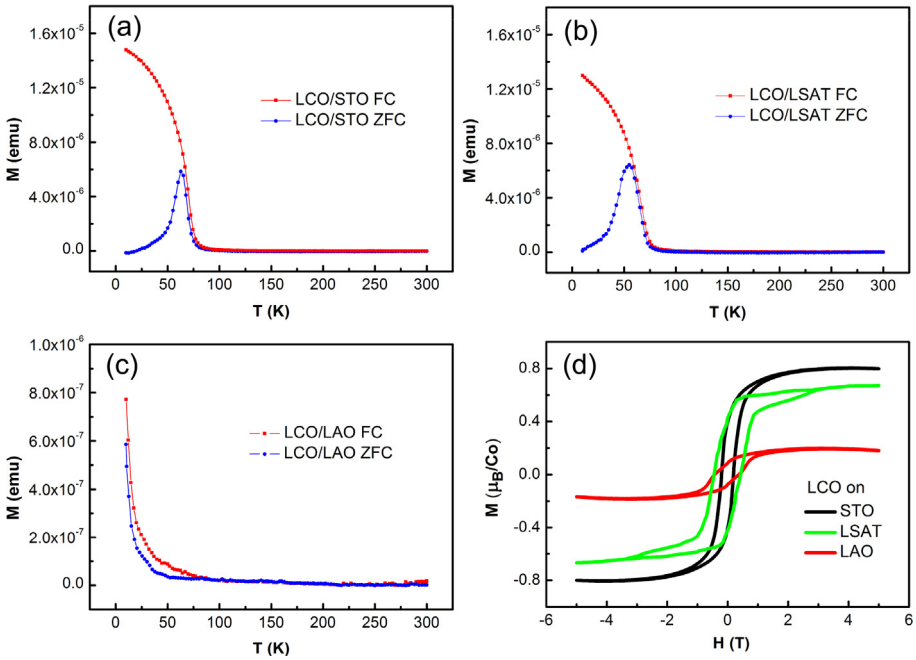

Fig. 8. Thermal magnetizations of the LCO/STO (a), LCO/LSAT (b) and LCO/LAO (c) films measured in both FC and ZFC modes with an applied field of 0.05 T. (b) Isothermal magnetizations of the LCO/STO, LCO/LSAT and LCO/LAO films, recorded at 10 K.

out-of-plane interatomic distances (green lines) from the HAADF images, as shown in Figs. 6(b) and 7(b). For the vertical domains, the out-of-plane La–La distances show more or less equal spacing (3.80 Å), whereas the in-plane La–La distances are 4.32 Å and 3.69 Å across dark and bright planes, respectively. Similarly, for the horizontal domains, the La–La distances along the direction of modulated structures in the dark stripes also show a lattice dilatation (4.44 Å versus 3.45 Å). The dilated atomic spacing indicates a lattice expansion in the LCO films, which can be attributed to the presence of oxygen vacancies in the films because the loss of O atoms can form larger Co^{2+} cations [36], and may increase the Coulomb repulsion between Co ions. The lattice expansion resulted from oxygen deficiency in the films can simultaneously make La atoms move further apart from each other, thus producing the dark stripes in the HRTEM images.

Based on the experimental results, we proposed atomic structure models for LCO, as shown in Figs. 6(c) and 7(c), respectively. To accommodate the observed modulations and in particular, to incorporate the $3a_0$ modulation, we constructed alternating one oxygen-deficient and two oxygen-stoichiometric unit cells along the modulation directions, with an oxygen vacancy content of 11%. Using the atomic structure models, we carried out systematic HRTEM image simulations. One simulated image with $\Delta f = -15.0$ nm (defocus value) and $t = 22.7$ nm (thickness) is shown in the inset of Fig. 6a, and the other one with $\Delta f = -15.0$ nm and $t = 24.6$ nm is displayed in the inset of Fig. 7(a). The white arrows indicate the positions of atomic columns with dark contrasts. From Figs. 6(a) and 7(a), it can be clearly seen that both simulated images agree well with the experimental ones. In the simulated images, the brightest features are columns of La and the next brightest features are columns of Co. It clearly shows that the intensity of pure Co^{2+} planes (containing oxygen vacancies) are weaker than that of Co^{2+}/Co^{3+} mixed planes. This corroborates that the dark stripes in the films originate from the oxygen vacancy ordering.

From the above microstructure analysis of three different films, a correlation can be found between the strain state of the film and the microstructure ordering. Both horizontally and vertically modulated structures are found in tensile-strained films, whereas only horizontally modulated structures are observed in compressive-strained films. For the films under tensile strain (LCO/STO and LCO/LSAT), the out-of-plane lattice parameter (c_{film}) decreases and the in-plane lattice parameters (a_{film} and b_{film}) increase in order to keep a same volume of the unit cell. This structural deformation reinforces the Jahn–Teller distortion induced by oxygen vacancy, which results in formation of the vertical domain structures. In our work, the appearance of both horizontal and vertical domain structures in the films under tensile strain is attributed to modulation direction change, which can partially relieve the interfacial strain. However, for compressive-strained film (LCO/LAO), lattice parameters of a_{film} and b_{film} decrease and lattice parameter of c_{film} increases. The structural deformation restrains the Jahn–Teller distortion, which leads to formation of horizontal domain structures.

The observed structural modulations are related to oxygen vacancies that lead to the existence of Co^{2+}. Both strain and oxygen vacancy in the LCO films can affect the spin states of Co ions, which is responsible for the ferromagnetic states. Fig. 8(a–c) shows the temperature dependent magnetization, M-T, of the LCO films, measured with an applied field of 0.05 T in FC and ZFC modes. Under our experimental conditions, the magnetization of the substrates is generally around -10^{-6} emu (not shown here), much lower than that of the LCO films. From Fig. 8(a–c), one can see that the FC and ZFC magnetization curves of all the three films are separated from each other at low temperature. For the ZFC curves of tensile-strained films, the magnetization reaches a maximum value at a temperature around 50–60 K, which usually represents a glass-like behavior [3]. Above a certain temperature, the ZFC curves begin to coincide with FC curves. The FC curves show a ferromagnetic-paramagnetic (FM-PM) transition, and the transition temperatures (T_c), defined by the inflection point in the FC curves, are 78 K and 75 K for the films under tensile strain and compressive strain, respectively. No evident change in T_c was found for the films grown on different substrates. Below T_c, these films exhibit ferromagnetic characteristics and above it they show a paramagnetic state, which is similar to FM-PM transition behavior of $La_{0.7}Sr_{0.3}CoO_3$ films [37]. However, the FM character is greatly weakened in the films under compressive strain. Fig. 8(d) shows

the magnetic field dependent magnetization, M-H, for LCO/STO, LCO/LSAT and LCO/LAO films measured with the field applied in the film plane at 10 K. The magnetism of the substrates shows a linear relation with the external magnetic field, whereas the magnetic moment of each film demonstrates hysteresis with the external magnetic field. It can be seen that the saturation magnetization (M_s) strongly depends on the strain state of the films. The saturation magnetization of the films grown under tensile strain is larger than that of the films grown under compressive strain. As tensile strain increases for films grown on STO, the M_s rises to 0.8 μ_B/Co.

Meanwhile, the presence of oxygen defects observed by HRTEM and HAADF suggests that the effect of microstructure must be taken into account. The XPS results show that there are a considerable number of oxygen vacancies and Co^{2+} ions, and the HRTEM images indicate that the oxygen vacancies are distributed throughout the films. The oxygen vacancy leads to the formation of Co^{2+} ions in the lattice, and the magnetization originates from the alternative arrangement of HS Co^{2+} ions and low-spin (LS) Co^{3+} ions. The enhanced ferromagnetic properties can be attributed to the interaction between structural deformation provoked by the strain and Jahn–Teller distortion of Co octahedra induced by oxygen vacancy. For the perpendicularly-modulated structures, the structural deformation reinforces the Jahn–Teller distortion (tetragonally-distorted Co octahedra). Thus, the HS Co^{2+} ions are stabilized and a long-range ferromagnetic ordering is enhanced. For the horizontally-modulated structures, the structural deformation is opposite to the Jahn–Teller distortion, which weakens the long-range ferromagnetic ordering. Note that no perpendicularly-modulated structure is found in the LCO film on LAO, and the magnetization of this film is worse than the other two films. Thus, the magnetization is positively correlated with the strain state, oxygen vacancy ordering and the content of perpendicularly-modulated structures.

4. Conclusions

In conclusion, LCO epitaxial films have been grown on different substrates by single target PLD. In the films under compressive strain, only horizontal domain structures were observed, whereas in the films under tensile strain, both horizontal and vertical domain structures were found. The change of domain direction, which is associated with the lattice mismatch and strain state in the film, can relax the strain in the LCO epitaxial films. XPS reveals the distribution of Co^{2+} and Co^{3+} ions, confirming the existence of oxygen vacancies in the LCO films. The simulated HRTEM images for LCO/STO reproduces the domain structures with dark stripes by introducing oxygen vacancies in the lattices. The saturated magnetization strongly depends on the strain state, oxygen vacancy and orientation of the domain structures in the epitaxial films. These results indicate the importance of lattice mismatch, oxygen vacancy and their independence in understanding the physical properties of cobalt-based oxides.

Acknowledgements

We would like to thank the financial support from the National Key Basic Research Development Program of China (Grant Nos.: 2012CB722705, 2013CB921700), the National Natural Science Foundation of China (Grant Nos.: 10974105 and 11520101002), and High-end Foreign Experts Recruitment Programs (Grant Nos.: GDW20143500163, GDW20163500110). Y. Q. Wang would also like to thank the financial support from the Taishan Scholar Program of Shandong Province, the Top-notch Innovative Talent Program of Qingdao City (Grant No.: 13-CX-08), and Qingdao International Center for Semiconductor Photoelectric Nanomaterials.

Appendix A. Supplementary data

Supplementary data associated with this article can be found, in the online version, at http://dx.doi.org/10.1016/j.apsusc.2017.06.315.

References

[1] P. Poizot, S. Laruelle, S. Grugeon, L. Dupont, J.M. Tarascon, Nano-sized transition-metal oxides as negative-electrode materials for lithium-ion batteries, Nature 407 (2000) 496–499.
[2] G. Briceño, H. Chang, X.D. Sun, P.G. Schultz, X.D. Xiang, A class of cobalt oxide magnetoresistance materials discovered with combinatorial synthesis, Science 270 (1995) 273–275.
[3] S.M. Zhou, L. Shi, J.Y. Zhao, L.F. He, H.P. Yang, S.M. Zhang, Ferromagnetism in $LaCoO_3$ nanoparticles, Phys. Rev. B 76 (2007) 172407.
[4] H. Hsu, P. Blaha, R.M. Wentzcovitch, Ferromagnetic insulating state in tensile-strained $LaCoO_3$ thin films from LDA+U calculations, Phys. Rev. B 85 (2012) 140404.
[5] S. Park, P. Ryan, E. Karapetrova, J.W. Kim, J.X. Ma, J. Shi, J.W. Freeland, W. Wu, Microscopic evidence of a strain-enhanced ferromagnetic state in $LaCoO_3$ thin films, Appl. Phys. Lett. 95 (2009) 072508.
[6] D. Fuchs, E. Arac, C. Pinta, S. Schuppler, R. Schneider, H.v. Löhneysen, Tuning the magnetic properties of $LaCoO_3$ thin films by epitaxial strain, Phys. Rev. B 77 (2008) 014434.
[7] A. Dubey, V.G. Sathe, R. Rawat, Signature of Jahn–Teller distortion and oxygen stoichiometry in Raman spectra of epitaxial $LaMnO_{3+\delta}$ thin films, J. Appl. Phys. 104 (2008) 113530.
[8] B. Liu, Y.Q. Wang, G.J. Liu, H.L. Feng, H.W. Yang, X.Y. Xue, J.R. Sun, Tuning the magnetic properties of $La_{0.67}Co_{0.33}O_{3-}\sigma$ films by oxygen pressure, Phys. Rev. B 93 (2016) 094421.
[9] B. Liu, G.J. Liu, H.L. Feng, C. Wang, H.W. Yang, Y.Q. Wang, Effect of oxygen vacancies on structural, electrical and magnetic properties of $La_{0.67}Sr_{0.33}CoO_3$ thin films, Mater. Des. 89 (2016) 715–720.
[10] B. Liu, Y.Q. Wang, G.J. Liu, H.L. Feng, H.W. Yang, J.R. Sun, Electrical transport properties of $La_{1-x}Sr_xCoO_3$ thin films, J. Appl. Phys. 120 (2016) 154103.
[11] F. Wang, Y.Q. Zhang, Y. Bai, W. Liu, H.R. Zhang, W.Y. Wang, S.K. Li, S. Ma, X.G. Zhao, J.R. Sun, Z.H. Wang, Z.J. Wang, Z.D. Zhang, Oxygen vacancy formation, crystal structures, and magnetic properties of three $SrMnO_{3-\delta}$ films, Appl. Phys. Lett. 109 (2016) 052403.
[12] H.Z. Guo, J.O. Wang, X. He, Z.Z. Yang, Q.H. Zhang, K.J. Jin, C. Ge, R.Q. Zhao, L. Gu, Y.Q. Feng, W.J. Zhou, X.L. Li, Q. Wan, M. He, C.H. Hong, Z.Y. Guo, C. Wang, H.B. Lu, K. Ibrahim, S. Meng, H. Yang, G.Z. Yang, The origin of oxygen vacancies controlling $La_{2/3}Sr_{1/3}MnO_3$ electronic and magnetic properties, Adv. Mater. Interfaces 3 (2016) 1500753.
[13] J.H. Kwon, W.S. Choi, Y.K. Kwon, R. Jung, J.M. Zuo, H.N. Lee, M. Kim, Nanoscale spin-state ordering in $LaCoO_3$ epitaxial thin films, Chem. Mater. 26 (2014) 2496–2501.
[14] O.H. Hansteen, H. Fjellvåg, B.C. Hauback, Crystal structure thermal and magnetic properties of $La_3Co_3O_8$. Phase relations for $LaCoO_{3-\delta}$ ($0.00 \leq \delta \leq 0.50$) at 673 K, J. Mater. Chem. 8 (1998) 2081–2088.
[15] R.F. Klie, Y. Ito, S. Stemmer, N.D. Browning, Observation of oxygen vacancy ordering and segregation in perovskite oxides, Ultramicroscopy 86 (2001) 289–302.
[16] A. Podlesnyak, S. Streule, J. Mesot, M. Medarde, E. Pomjakushina, K. Conder, A. Tanaka, M. Haverkort, D. Khomskii, Spin-state transition in $LaCoO_3$: direct neutron spectroscopic evidence of excited magnetic states, Phys. Rev. Lett. 97 (2006) 247208.
[17] R.F. Klie, J.C. Zheng, Y. Zhu, M. Varela, J. Wu, C. Leighton, Direct measurement of the low-temperature spin-state transition in $LaCoO_3$, Phys. Rev. Lett. 99 (2007) 047203.
[18] D. Fuchs, C. Pinta, T. Schwarz, P. Schweiss, P. Nagel, S. Schuppler, R. Schneider, M. Merz, G. Roth, H.v. Löhneysen, Ferromagnetism order in epitaxially strained $LaCoO_3$ thin films, Phys. Rev. B 75 (2007) 144402.
[19] W.S. Choi, J.H. Kwon, H. Jeen, J.E. Hamann-Borrero, A. Radi, S. Macke, R. Sutarto, F. He, G.A. Sawatzky, V. Hinkov, M. Kim, H.N. Lee, Strain-induced spin states in atomically ordered cobaltites, Nano Lett. 12 (2012) 4966–4970.
[20] N. Biškup, J. Salafranca, V. Mehta, M.P. Oxley, Y. Suzuki, S.J. Pennycook, S.T. Pantelides, M. Varela, Insulating ferromagnetic $LaCoO_{3-\delta}$ films: a phase induced by ordering of oxygen vacancies, Phys. Rev. Lett. 112 (2014) 087202.
[21] V.V. Mehta, N. Biškup, C. Jenkins, E. Arenholz, M. Varela, Y. Suzuki, Long-range ferromagnetic order in $LaCoO_{3-\delta}$ epitaxial films due to the interplay of epitaxial strain and oxygen vacancy ordering, Phys. Rev. B 91 (2015) 144418.
[22] G. Van Tendeloo, O.I. Lebedev, M. Hervieu, B. Raveau, Structure and microstructure of colossal magnetoresistant materials, Rep. Prog. Phys. 67 (2004) 1315–1365.
[23] J. Gazquez, S. Bose, M. Sharma, M.A. Torija, S.J. Pennycook, C. Leighton, M. Varela, Lattice mismatch accommodation via oxygen vacancy ordering in epitaxial $La_{0.5}Sr_{0.5}CoO_{3-\delta}$ thin films, APL Mater. 1 (2013) 012105.
[24] M.A. Torija, M. Sharma, M.R. Fitzsimmons, M. Varela, C. Leighton, Epitaxial $La_{0.5}Sr_{0.5}CoO_3$ thin films: structure, magnetism, and transport, J. Appl. Phys. 104 (2008) 023901.

[25] P.E. Vullum, R. Holmestad, H.L. Lein, J. Mastin, M.-A. Einarsrud, T. Grande, Monoclinic ferroelastic domains in $LaCoO_3$-based perovskites, Adv. Mater. 19 (2007) 4399–4403.
[26] P.E. Vullum, H.L. Lein, M.-A. Einarsrud, T. Grande, R. Holmestad, TEM observations of rhombohedral and monoclinic domains in $LaCoO_3$-based ceramics, Philos. Mag. 88 (2008) 1187–1208.
[27] M.M. Natile, E. Ugel, C. Maccato, A. Glisenti, $LaCoO_3$: effect of synthesis conditions on properties and reactivity, Appl. Catal. B: Environ. 72 (2007) 351–362.
[28] R. Brackmann, C.A. Perez, M. Schmal, $LaCoO_3$ perovskite on ceramic monoliths-pre and post reaction analyses of the partial oxidation of methane, Int. J. Hydrogen Energy 39 (2014) 13991–14007.
[29] A. Chainani, M. Mathew, D.D. Sarma, Electron-spectroscopy study of the semiconductor-metal transition in $La_{1-x}Sr_xCoO_3$, Phys. Rev. B 46 (1992) 9976–9983.
[30] J.F. Moulder, W.F. Stickle, P.E. Sobol, K.D. Bomben, A reference book of standard spectra for identification and interpretation of XPS data, in: J. Chastain, R.C. King Jr (Eds.), Handbook of X-Ray Photoelectron Spectroscopy, Perkin-Elmer Corporation, Physical Electronics Division, Eden Prairie, Minnesota, USA, 1995, pp. 82–83.
[31] B. Dalal, B. Sarkar, V.D. Ashok, S.K. De, Structural, electric and magnetic properties of $La_{1-x}Sr_xCo_{1-x}Ru_xO_3$ ($0 \le x \le 0.6$) solid solution, J. Alloys Compd. 649 (2015) 1164–1173.
[32] M.A. Langell, M.D. Anderson, G.A. Carson, L. Peng, S. Smith, Valence-band electronic structure of Co_3O_4 epitaxy on CoO (100), Phys. Rev. B 59 (1999) 4791–4798.
[33] S. Sonsupap, P. Kidkhunthod, N. Chanlek, S. Pinitsoontorn, S. Maensiri, Fabrication structure, and magnetic properties of electrospun $Ce_{0.96}Fe_{0.04}O_2$ nanofibers, Appl. Surf. Sci. 380 (2016) 16–22.
[34] D.O. Klenov, W. Donner, B. Foran, S. Stemmer, Impact of stress on oxygen vacancy ordering in epitaxial $(La_{0.5}Sr_{0.5})CoO_{3-\delta}$ thin films, Appl. Phys. Lett. 82 (2003) 3427–3429.
[35] Z.L. Wang, J.S. Yin, Cobalt valence and crystal structure of $La_{0.5}Sr_{0.5}CoO_{2.25}$, Philos. Mag. B 77 (1998) 49–65.
[36] V.V. Mehta, M. Liberati, F.J. Wong, R.V. Chopdekar, E. Arenholz, Y. Suzuki, Ferromagnetism in tetragonally distorted $LaCoO_3$ thin films, J. Appl. Phys. 105 (2009) 07E503.
[37] Z. Othmen, A. Schulman, K. Daoudi, M. Boudard, C. Acha, H. Roussel, M. Oueslati, T. Tsuchiya, Structural, electrical and magnetic properties of epitaxial $La_{0.7}Sr_{0.3}CoO_3$ thin films grown on $SrTiO_3$ and $LaAlO_3$ substrates, Appl. Surf. Sci. 306 (2014) 60–65.